RSC Advances

AFM study of asphalt binder "bee" structures: Origin, mechanical fracture, topological evolution, and experimental artifacts

Journal:	*RSC Advances*
Manuscript ID	RA-ART-07-2015-013982.R1
Article Type:	Paper
Date Submitted by the Author:	12-Oct-2015
Complete List of Authors:	Hung, Albert; North Carolina A&T State University, Nanoengineering Fini, Elham; North Carolina A&T State University, Civil, Architectural and Environmental Engineering
Subject area & keyword:	Materials < Physical

AFM study of asphalt binder "bee" structures: Origin, mechanical fracture, topological evolution, and experimental artifacts

Albert M. Hung[a] and Elham H. Fini[b]

[a.] Department of Nanoengineering, Joint School of Nanoscience and Nanoengineering, North Carolina A&T State University, Greensboro, NC 27401
[b.] Department of Civil, Architectural and Environmental Engineering, North Carolina A&T State University, Greensboro, NC 27411

Electronic Supplementary Information (ESI) available: additional figures and text describing experimental method, image analysis, and AFM imaging artifacts. See DOI: 10.1039/x0xx00000x

The morphology of "bee" structures on the surface of bituminous asphalt binder was studied by AFM microscopy to provide insight into their origin. Based on how the "bees" flattened and fractured under applied tensile strain, the "bee" structures were hypothesized to be the result of wrinkling of very thin surface films on the order of 10 nm thick. Theories of thin film deformation suggest that the wavelength and amplitude of the "bees" may be related to the stiffness and thermal expansion coefficient of the bitumen. The study also showed that "bee" structures exhibited topological evolution over time depending on humidity and temperature in a manner consistent with the idea of the "bees" being composed of crystallized hydrophobic wax. The results of this paper should contribute to a better understanding of the relation between "bee" structures and bituminous material properties.

1. Introduction

Bitumen or asphalt binder is a hydrocarbon-based material, typically a product of petroleum crude oil refineries that is used as a viscoelastic glue to bind aggregates and fillers together to form asphalt concrete. Environmental, economic, and political concerns over the depletion, increased cost, and foreign sourcing of non-renewable petroleum resources has spurred interest in developing renewable alternatives and recycling of bitumen. While performance-based metrics can provide an empirical method to evaluate qualification of alternative materials, a fundamental understanding of the interaction between binder chemical composition, microstructure, and performance is necessary for both selecting valid metrics and guiding new material development.

Loeber *et al*. were the first to investigate the microscopic surface topography of bitumen samples and reported "bee-like" structures: elongated regions with transverse stripes of high and low surface height.[1] The structure is sometimes referred to as *catana phase*, and it is typically surrounded by a flat *peri phase* region that is itself surrounded by a mechanically distinct *para* or *para phase* area.[2, 3] Figure 1 shows an example image of the microstructures, and the aforementioned terminologies are used herein. As shorthand, "bee" structure is used to refer to the catana and peri phase combined as a single unit. The "bees" were thought to consist of asphaltenes,[1, 4-6] a heterogeneous mixture of polycyclic aromatics and metalloporphorines that is insoluble in *n*-heptane. This assertion was based on an observed correlation between increased asphaltene content and the occurrence of "bee" structures. Another study implicated the transition metal cations typically associated with the asphaltenes in "bee" formation.[2] However,

some bitumens still showed "bees" after asphaltenes were removed, and correlation of endothermic peaks in DSC with morphological evolution has given weight to alternative hypotheses that the "bees" are composed of crystalline paraffin wax (predominantly linear *n*-alkanes) or microcrystalline wax (naphthenes and *iso*-alkanes).[7-12] More complex theories propose that both wax and other bitumen components are responsible for the "bee" structures *via* co-crystallization, heterogeneous nucleation, or other interaction.[12-15]

In addition to chemical composition, questions remain as to the origin, properties, and subsurface structure of these features as well as their relation to material performance. Neutron scattering and rheological measurements demonstrated that a wax-based heterogeneous microstructure can develop in the bulk with possible relation to the surface microstructure.[12, 16] Freeze-fracture experiments also suggested the possibility of a deeper microstructure for the "bees,"[17] although moisture condensation on the frozen surface may have been responsible for the observed structures given that water is known to alter the surface texture of bitumen.[18] An alternative theory is that the "bee" structures do not have significant depth but instead are thin films of wax that crystallize on the surface of the bitumen as it cools down from the casting temperature to the ambient temperature.[19-21] It has been well-documented that both polyethylene and paraffin can crystallize as thin lamellar sheets.[22-26] Polyethylene single crystals may even exhibit shield-shaped or rippled morphologies that bear some resemblance to the "bees."[22, 23]

Recently, Nahar *et al*.[19] and Lyne *et al*.[20] both proposed that the "bee" structures are stiff surface films that wrinkle under some form of native compressive strain. An approximate value of 70 to 140 nm was calculated for the film thickness.[20] We independently arrived at a similar idea based on knowledge of unrelated work with wrinkled silicon films for flexible electronics.[27] Theoretical models describing the deformation of stiff, elastic thin films on compliant or viscoelastic substrates are well developed.[27-30] We hypothesized that if this model was correct, then an applied tensile strain should preferentially "un-wrinkle" the "bees" aligned parallel to the stretching direction. With increasing tensile strain, cracks appear in the peri phase,[31, 32] and the depth of the cracks may be a direct measurement of the purported film thickness. The "wrinkled film" model also predicts that the wavelength and amplitude of the "bee" structures are indicative of material properties,[27] and the structures may not be stress-free but subject to creep over time.[28-30] In this paper, we report the results and analysis of an AFM study showing strain-induced flattening and fracture of bitumen "bee" structures. In addition, we study how the bitumen surface texture evolves over the course of several days depending on humidity and temperature. The physical origin of the "bee" structures and experimental artifacts encountered during this study are discussed in detail. A better fundamental understanding of the "bee" structures may offer insight into the molecular basis of bitumen mechanical properties and their evolution with time as the material ages.[33-35]

2. Experimental Methods

The base asphalt used in this study was PG 64-22 asphalt commonly used in the United States acquired from Associated Asphalt Inc. (http://associatedasphalt.com). Table 1 provides the SARA fractions and some properties of this bitumen. The crystallized wax fraction was too small to be determined by DSC. A typical sample was made by lightly heating the stock in order to transfer a small amount of bitumen onto glass slides. The samples were annealed at 150°C for at least 30 min then placed in a fume hood to cool under ambient conditions for at least 1 hr, although the samples typically reached below 30 °C within 10 min. AFM imaging was typically

performed within a day of annealing. The samples were imaged with a large stage 5600LS AFM (Keysight Technologies) in tapping mode with TAP-300 silicon cantilever tips (Budget Sensors, 40 N/m nominal spring constant, 300 kHz nominal frequency). The amplitude setpoint was often kept above 75% of the reference amplitude to reduce tip-sample pressure. Images were processed and analyzed with Gwyddion and ImageJ open-source software.

Table 1. Properties of PG 64-22 asphalt binder.

Property		SARA fraction	%
Specific Gravity at 15.6 °C	1.039	Saturates (aliphatic)	9.3
Flash Point, Cleveland Open Cup, °C	335	Aromatics (naphthene)	44
Change in Mass, RTFO	-0.0129	Resins (polar aromatic)	39.9
Absolute Viscosity at 60 °C, Pa·s	202	Asphaltenes	6.8

While true in situ imaging of samples during stretching was not done, it is possible on the large stage 5600LS to implement a simple mechanical deformation setup and relocate previously scanned locations on the sample to obtain "before" and "after" pictures for direct comparison. For this experiment, a bitumen sample was cast over two glass slides that were set side-by-side against each other (see Electronic Supplementary Information, ESI Figure S1). Strain is applied by placing a spacer under the crack between the slides, thus opening the crack and stretching a portion of the bitumen sample that remains suspended over the opening. The bitumen film is 0.5-1 mm thick, and the strain is applied incrementally to avoid high strain rates. In order to repeatedly find and image the same location on a given sample, the sample was marked with dry silver paint dust and a picture was taken through the AFM optical camera so that the tip could be repositioned over the same area with 20 μm accuracy. A 40 μm scan of the area of interest is taken at the start of the experiment. Subsequent 20 μm scans are compared to the larger image to determine the exact position of the tip on the sample surface and make adjustments as necessary. Analysis of the "before" and "after" pictures assuming plane strain with a correction for incidental sample rotation gives a measure of true strain and the angle of the principle strain axis (see ESI section S.2 for procedure and figures).

3. Results and Discussion

3.1 AFM of "bee" structures under applied tensile strain

In the "wrinkled film" hypothesis, the "bee" structures arise from a chemically and mechanically distinct surface film that separates from the bulk bitumen.[24, 25] A difference in thermal contraction between the two phases during cooling results in a native compressive strain on the film, and at a critical compressive strain the film buckles into periodic ripples as schematically illustrated in Figure 1. If the "bees" are a result of compressive strain, then tensile strain should "un-wrinkle" the "bees," especially the ones oriented parallel to the stretching direction. Jahangir *et al*. showed a reduction in the catana phase area at 5% average strain as well as some crack initiation between individual peri phase regions, but they reported the "bee" structures remained intact.[36] Both Nahar et al.[32] and Fischer and Dillingh[31] also reported a reduction in the catana phase area upon stretching, but no mention was made of whether parallel-aligned "bees" flattened first. Cracking of the peri phase was observed at higher applied strain,

but the cracks did not appear very deep, a fact that was attributed to either rapid filling of the crack by fluid para phase[31] or the cracks initiating as crazes.[32]

When large strains are applied to soft bitumen samples, plastic deformation phenomena like necking and shear banding can concentrate most of the strain in small regions of the sample. As a result, the distribution of applied strain might vary widely across the sample area, making it difficult to correlate AFM images to exact strain levels and defeating the purpose of mechanisms designed to apply strain in a controlled fashion. Therefore, we attempted an alternative method in which the exact same area of the sample was imaged before and after the sample was stretched. The magnitude and orientation of the applied strain localized in that specific area was calculated from the "before" and "after" images so that mechanical deformation could be accurately correlated to its effect on the sample without the need for a controlled setup to apply strain (see ESI section S.2).

In Figure 2, AFM images of a bitumen sample before and after stretching showed significant alterations to the "bee" structures. The overall stretching direction was horizontal, but in the imaged area the local applied tensile strain due to the stretching was measured at 7.4% and angled up at 24°, a significant deviation in orientation from the average. The catana phase structures oriented parallel to the local applied strain direction were mostly eliminated whereas those structures oriented perpendicular to the strain direction suffered milder reductions in amplitude (height) and area. Fast Fourier transform (FFT) analysis of the images corroborated these observations. The FFT showed that a large portion of the "bees" were oriented at an angle to the horizontal before stretching (Fig. 2a, inset, yellow arrow), and those "bees" selectively disappeared after stretching (Fig. 2b, inset, yellow arrow). In fact, that predominance of "bees" oriented off-horizontal initially may have caused the local applied strain to deviate so far in orientation. ImageJ was used to identify 91 points in the images (Fig. 2c, blue crosses) and measure how far they displaced after stretching (Fig. 2d, red crosses). Comparison of the real displacements to predicted displacements based on a uniform plane strain (Fig. 2d, green circles) indicated that the para phase areas between "bee" structures experienced greater than average applied strain and that the para phase was much softer than the peri and catana phases.

The "bee" structures remained intact at 7.4% strain, but images shown in Figure 3 taken from another location on the same sample revealed crack initiation. The applied strain in this area is unknown because our method of calculating strain required the acquisition of a "before" image of an area. It was difficult to predict locations of strain concentration prior to stretching, and severe deformation hindered identification of previously imaged locations. However, based on the degree of flattening and fracturing of the "bee" structures, the area shown in Fig. 3 was likely subject to much higher strain than the area shown in Fig. 2. Most of the catana phase disappeared and was barely distinguishable from peri phase. Significant fracturing of the "bee" structures was evident in the images. For example, the inset in Fig. 3 highlights what appears to be a "bee" structure split in half by a single vertical crack. The elliptical peri phase shape and residual catana phase on the right half suggests that the long axis of the original structure was oriented horizontally. However, the left half shows a vertical wrinkle pattern along the crack edge that may be due to buckling under transverse strain similar to what occurs for thin polymer sheets.[37]

According to our hypothesis, if the "bee" structure is a wrinkled thin film, then a crack in the film could be as deep as the film thickness. The crack should also reveal the material underneath the film, material that is predicted to be identical to para phase material. The crack depth could not be accurately measured, but it appeared to be very shallow, possibly on the order

of 10 nm as shown by the line profile plots in Fig. 3. Accurate measurement of the peri phase film thickness was hindered by shear-induced dilation of the bitumen[38] and tip oscillation artifact or "ringing." This artifact may have been a result of stronger adhesion of the tip to the para phase compared to the peri phase.[39, 40] The profile plots in Fig. 3 show that ringing occurred while scanning over para phase areas as well as cracks in the peri phase, suggesting a similarity between the two areas. Also, wherever a crack met the para phase, no distinct border or discontinuity was seen between the two regions. These observations support the idea that cracks in the "bees" exposed material identical to para phase material that was beneath the film.

AFM microscopy alone cannot verify the material composition, therefore a counter argument could be that the material in the cracks is peri phase that has undergone load-induce phase transformation, molecular reorganization, or plastic deformation similar to crazing of stretched polymers.[26] However, such a process would consume the peri phase as the crack widened and change the outline of the crack edges until they lose coherence. As can be seen in Fig. 3, the edges of the crack seem pristine as if the "bees" could be reassembled like a jigsaw puzzle, and the peri phase area does not appear significantly depleted. Another counter argument is that the para phase is fluid enough to immediately fill in the cracks.[31] However, many of the cracks are 50 nm wide or less, so the para phase would have to be exceptionally fluid to wick up such a narrow channel if the cracks were 100 nm or deeper. Furthermore, the larger cracks do appear as shallow valleys in Fig. 3 and don't immediately fill in. Therefore, the counter arguments cannot be supported based on our observations.

3.2 The origin of "bee" structures as wrinkled thin films

The images in Figure 3 of flattened and fractured "bees" give a strong visual impression that the "bees" are primarily surface structures and not bulk structures. The data is consistent with the hypothesis that the "bees" are wrinkled, stiff thin films of crystallized paraffin wax supported by a compliant substrate,[19-21] but more can be done to refine this hypothesis and elaborate on its implications, especially if the film is on the order of 10 nm thick as suggested by the AFM results discussed above. The Huang group and others have reported theoretical modelling and experimental verification of the mechanical deformation of thin, stiff films laminated on soft or viscoelastic substrates.[27-30] When such a system is subjected to a lateral compressive strain ε_{load}, the stiff film is less able to support the strain than the soft substrate. If ε_{load} exceeds a critical compressive strain ε_c, the film buckles and transforms some of the lateral compressive strain into bending and normal strain in order to reduce the total elastic strain energy.[27-30] Unless the film delaminates from the substrate, the thin film buckles into highly regular, sinusoidal wrinkles with specific wavelength λ_o and amplitude A_o. The values of λ_o and A_o depend on the film thickness h and the plane-strain moduli of the film $\bar{E}_f$ and the substrate $\bar{E}_s$ (plane-strain modulus $\bar{E} = E/(1-\nu^2)$, where E is Young's modulus and ν is Poisson's ratio).[27-30] Applying this model to the "bee" structures, we replace ε_{load} with ε_{bee}: the native compressive strain that is purported to cause the wax thin film to wrinkle into "bees." ε_{bee} is thought to arise naturally from curvature elastic strain of a paraffin single crystal[21-23] or a difference in thermal contraction between the wax film and the resin substrate.[20] In the limit of small deformations, λ_o and A_o are given by the following equations:[27-30]

$$\lambda_o = 2\pi h \left(\frac{\bar{E}_f}{3\bar{E}_s}\right)^{1/3} = \frac{\pi h}{\sqrt{\varepsilon_c}} \quad (1)$$

$$A_o = h\sqrt{\frac{\varepsilon_{\text{bee}}}{\varepsilon_c} - 1} \quad (2)$$

$$\varepsilon_c = \frac{1}{4}\left(\frac{3\bar{E}_s}{\bar{E}_f}\right)^{2/3} \quad (3)$$

Based on this model, initial growth of the "bee" structures is hypothesized to follow three stages as illustrated schematically in Fig. 1: film nucleation, film growth and thermal contraction, and film buckling. During nucleation, chemical constituents believed to be paraffin wax separate from the bitumen melt and crystallize as a thin film at the surface (Fig. 1a). The center of the film is placed under increasing compressive stress due to thermal contraction of the bitumen as it cools down (Fig. 1b). When the compressive strain ε_{bee} exceeds the critical strain ε_c, the film buckles into sinusoidal wrinkles (Fig. 1c). Buckling can initiate before the sample is completely cooled and while the surface film continues to grow. Any film growth that occurs at later stages of cooling is subject to less total strain, and buckling doesn't occur for $\varepsilon_{\text{bee}} < \varepsilon_c$. Thus, the peri phase is the same material as the catana phase but under less compressive strain and unwrinkled.

Lyne *et al*. used Equation 1 to calculate an estimate of 70 – 140 nm for the film thickness of the "bees" based on PeakForce QNM™ (quantitative nano-mechanical property mapping) measurements that reported the modulus of both phases to have similar values around 30 MPa with the film being slightly stiffer.[20] However, assuming no difference in Poisson's ratio v between the film and the substrate, those numbers lead to a value of $\bar{E}_f/3\bar{E}_s \approx 1$ and a critical buckling strain of $\varepsilon_c = 25$ % which seems unrealistic. Other studies employing QNM,[41, 42] nano-indentation,[43] or micro-rheology[36, 44] have each reported widely differing values in the range of 0.3 – 5 GPa for the elastic or instantaneous modulus of the para phase. Most of these reports show the peri phase to be stiffer than the para phase by up to a factor of two,[41, 42, 44] and a few studies show the para phase to be stiffer.[36] But, if the peri phase is only 10 nm thick, indentation-type mechanical measurements may not directly measure the compression modulus of the film but a convolution of the compression modulus of the underlying substrate and the bending and tensile moduli of the film, perhaps resulting in much of the variation in the reported data for the mechanical properties of the peri and catana phases. For ε_c to be of a reasonable value, the peri phase should be significantly stiffer than the para phase ($\bar{E}_f \gg \bar{E}_s$), consistent with image analysis of Fig. 2d.

We assume that the difference in Poisson's ratio v between the film and substrate is negligible, so the ratio of the plane-strain moduli of the two phases $\bar{E}_f/\bar{E}_s$ is equal to the ratio of the Young's moduli. Selecting appropriate values for $\bar{E}_f$ and $\bar{E}_s$ to apply to the above equations requires consideration of both the experimental data and the theoretical model. Work by Huang and Im[28] states that for a viscoelastic substrate, the applicable value of $\bar{E}_s$ is the time-dependent relaxation modulus or the equilibrium relaxation modulus if the system reaches equilibrium. The substrate material is thought to be para phase and probably is the majority material component of bitumen which dominates bulk properties. Both micro- and macroscale measurements typically give the equilibrium relaxation modulus to be in the range of 0.1 – 10 MPa.[36, 44, 45] Conversely, if the film is crystallized paraffin wax then it is not unreasonable to expect $\bar{E}_f$ to be close to that for high-density polyethylene. For comparison, the transverse modulus of draw-aligned linear polyethylene fibers is measured to be 3-9 GPa[46, 47] which is the same order of magnitude as the highest reported values of instantaneous elastic modulus for the "bee" structures at 2-5 GPa.[36, 43] Jahangir *et al*. performed AFM indentation creep measurements and calculated viscoelastic parameters based on fitting to the three-parameter Voigt model.[36] For two different bitumen

samples (AAD and BI0002), they reported values for the equilibrium relaxation modulus of the para phase to be 0.09 and 9 MPa and the instantaneous modulus of the peri phase to be 2.5 and 4.1 GPa, respectively. Applying those numbers for $\bar{E}_s$ and $\bar{E}_f$, the thickness h is calculated to be 3-13 nm given λ_o = 450 nm as measured in our study (see ESI Figure S6). Very preliminary measurements on PG 64-22 binder gives $\bar{E}_f/\bar{E}_s \sim 10^4$ and $h \approx 5$ nm (see ESI Figure S7). Note that a factor of 8 difference in $\bar{E}_f/\bar{E}_s$ yields a difference in h of only a factor of 2. These calculations for the film thickness h are intended to be merely order-of-magnitude estimates, yet h = 10 nm correlates well with AFM measurements of paraffin wax which showed a layered morphology of stacked sheets 3-30 nm thick with 4-8 nm being most common.[24, 25] Similarly, polyethylene crystals were observed with a layer thickness of 12-15 nm.[23] Dourado *et al*.[43] also reported increasing stiffness and hardness with decreasing indentation depth less than 10 nm in their nano-indentation measurement of 50/70 penetration grade binder. They very briefly posited that this "surface hardening" effect could be related to either oxidation or phase separation at the surface.

Combining Equations 1 and 2, the magnitude of the native compressive strain ε_{bee} that creates the wrinkled "bees" can be calculated from a measurement of the ratio A_o/λ_o:

$$\varepsilon_{\text{bee}} = \left(\pi \frac{A_o}{\lambda_o}\right)^2 + \varepsilon_{\text{c}} \quad (4)$$

Measurements from AFM images give a maximum value around 0.05 for the ratio A_o/λ_o. Thus, using the same values for modulus as above, ε_{c} is calculated to be 0.057-0.88 %, and the maximum ε_{bee} is 2.5-3.3 %. Although more sophisticated models are available, the small deformation approximation is believed to be sufficiently accurate at values of $A_o/\lambda_o \approx 0.05$ and $\varepsilon_{\text{bee}} \approx 3$ %.[27] Note that an applied tensile strain of 7.4 % as in Fig. 2 is greater than ε_{bee} and should flatten the "bees," but some structures may not completely flatten due to microscale variation in the distribution of the applied strain. The estimate of $\varepsilon_{\text{bee}} \approx 3$ % is a reasonable order of magnitude and helps validate the "wrinkled film" hypothesis as a realistic possibility.

If ε_{bee} is the result of differential thermal contraction upon cooling, then it is also instructive to calculate an estimate of this thermal strain $\varepsilon_{\text{thermal}}$ for comparison:

$$\varepsilon_{\text{thermal}} = \Delta\alpha_L \Delta T \quad (5)$$

where $\Delta\alpha_L = \alpha_{sub} - \alpha_{film}$ is the difference in linear thermal expansion coefficient between the substrate and film material and $\Delta T = T_N - T_{room}$ is the difference between the temperature at which the film nucleates and room temperature. Given approximations of 60 °C for ΔT and 2×10^{-4} °C^{-1} and 1×10^{-4} °C^{-1} for the linear thermal expansion coefficients of bitumen and polyethylene, respectively,[10, 15, 16, 48, 49] $\varepsilon_{\text{thermal}}$ is calculated as 0.6 %. Polyethylene crystals are not perfectly flat but possess a 3-dimensional morphology resulting in curvature elastic strain that is a probable source of additional strain.[21-23] If the contribution of curvature can be accounted for in the calculation of ε_{bee}, then the amplitude to wavelength ratio A_o/λ_o may be a useful indicator of the thermal expansion coefficient of bitumen.

Both wavelength λ_o and amplitude A_o should decrease as the substrate becomes harder with aging, and preliminary data appears to follow this trend.[35] In this model, A_o is also a function of the compressive strain $\varepsilon_{\text{load}}$ whereas λ_o is not. If the surface film is comprised of a similar chemical species across different bitumen sources, then $\bar{E}_f$ and h may not vary significantly, and thus a measurement of λ_o could be used as an indicator of bitumen stiffness $\bar{E}_s$.

The lack of accurate values for h and $\bar{E}_f$ means that a measure of λ_o cannot be used to quantitatively calculate $\bar{E}_s$, but it may yet be useful as a qualitative figure of merit. Furthermore,

the local variation in λ_o over a given area may provide valuable information about the specified sample. This variation could be the result of a proportional variation in film thickness h and be indicative of the molecular weight distribution of the film constituents (e.g. paraffin wax). A broad distribution in λ_o may also be due to rapid cooling which kinetically traps non-equilibrium deformation modes. This in turn could indicate that samples have not been annealed to their equilibrium state.

3.3 Time, temperature, and humidity-dependent topological evolution

Another implication of the "wrinkled film" hypothesis is that the "bee" structures are not entirely stress-free. The wrinkling effect relaxes in-plane stress while introducing bending stress in the film and normal stress in the substrate. These stresses may further confound AFM measurement of the mechanical properties of the "bees." The catana phase in particular could exhibit large variability since the material in the low (dark) regions is under compression while the tall (light) regions are under tension.

Residual stresses can also result in time-dependent topological evolution of the "bee" structures due to creep and relaxation. Huang and co-workers reported theory and modelling of the mechanical deformation of stiff, elastic thin films laminated on soft, viscoelastic substrates and subjected to an instantaneous compression.[28-30] They predicted wrinkling of the thin film developing over time in three stages: initial growth, coarsening, and equilibrium.[28] During initial growth, the viscoelastic substrate responds like a stiff glass to the rapid deformation, and λ and A of the wrinkled thin film exhibit lower values because the effective substrate stiffness $\bar{E}_s$ is the instantaneous modulus. After initial growth, the viscoelastic substrate responds like a soft rubber over long timescales, and the wrinkles coarsen due to creep and relaxation. $\bar{E}_s$ decreases, towards the value of the equilibrium relaxation modulus, resulting in λ and A increasing over time until they reach equilibrium values.[28] The "bees" may coarsen similarly, but because they assemble from cooling of soft, molten bitumen instead of as a result of instantaneous compression, the initial values of λ and A and their path to equilibrium are different. The timescale for coarsening is also an important consideration. Viscoelastic polymers can exhibit multiple creep decay time constants reflecting different characteristic modes of molecular rearrangement in the material.[26]

The possibility of topological evolution over time led to the design of a more detailed study on the effect of both storage temperature and relative humidity on surface morphology. Figure 4 shows AFM images of three samples stored either under ambient conditions in a covered petri dish (22 °C and *ca*. 50 % relative humidity), at room temperature in dry air (22 °C in a tightly capped jar with Drierite dessicant), or at 4 °C in dry air. Each sample was repeatedly imaged at the exact same location every 3-7 days over the course of 32 days. The sample stored under ambient conditions of temperature and humidity showed the most dramatic change where the para phase between the "bees" expanded vertically. Immediately after high-temperature annealing the samples likely had little if any water content, but the AFM images suggest that atmospheric water might have absorbed into at least the top layer of bitumen over time, especially in the para phase region. Dos Santos *et al*. showed how water immersion significantly altered the surface morphology of bitumen,[18] and Fig. 4b shows some similarities to the water-altered textures they observed. Although FTIR gave no evidence of water absorption, the amount of water may have been too small to be detected, especially if band broadening due to hydrogen bonding spread out the peaks.[50] Water absorption would also imply that the para phase is composed of more polar materials while the "bees" themselves are non-polar and hydrophobic

which might even reduce water absorption. Variations in chemical polarity on the microstructured surface have also been observed by chemical force microscopy.[51]

For each sample, the maximum amplitude (the difference between maximum and minimum height within the catana phase, divided by two) for 20 to 30 "bees" within the selected image area was measured and individually tracked through the duration of the experiment. The average increase in maximum amplitude over time is plotted in Figure 5. In the aforementioned three samples, the average maximum amplitude of the "bees" was in the range of 17-24 nm and had increased 8.5-17 % after 32 days. Most of that increase occurred within the first few days after casting the sample, although this trend was found to be slower for the sample stored at 4 °C compared to those stored at room temperature. These data are consistent with our prediction of wrinkle coarsening as the effective $\bar{E}_s$ decreases and approaches the equilibrium relaxation modulus.

To further study the evolution of the "bees" when conditioned in various environments, the wavelength of the "bees" was measured by a different method of FFT analysis (see ESI Figure S6) instead of individual "bee" tracking. One data point per image was obtained giving the predominant wavelength among all structures in the image. Even though some trends in the change of wavelength over time were observed, more data are required before definitive conclusions can be drawn.

As discussed above, the model of the "bees" as wrinkled surface films suggests that creep and relaxation of the underlying viscoelastic bitumen can occur, resulting in coarsening as λ and A approach an equilibrium limit. Jahangir *et al*. gave creep decay time constants of 1.5 min and 13 min based on micro-rheology measurements for BI0002 and AAD binders, respectively.[36] Our data suggest the possibility of another decay constant on the order of 1-2 days during which coarsening continues. In the case of samples stored at room temperature, the amplitudes also appeared to shrink slightly after longer times, indicating the possibility of further evolution proceeding on the timescale of a few months. The origin of these decay constants is unknown and warrant further investigation as they may each represent a different molecular rearrangement or aging process in the material.[26]

Surfaces are typically high-energy areas, and chemical species of lower surface energy such as non-polar hydrocarbons tend to segregate to and passivate the surface to reduce the total free energy.[52] This effect is driven by thermodynamic principles; thermal gradients or solvent diffusion do not necessarily control its occurrence. Long-chain linear *n*-alkanes (paraffins) are a likely candidate for the composition of the surface films because they have lower surface energy than polar or aromatic compounds. They also have lower solubility, higher crystallinity, and higher melting temperatures than short-chain, branched, or unsaturated hydrocarbons. However, this assertion is not without controversy as "bee" structures showed some correlation with higher concentrations of asphaltenes or metal cations, and the addition of more polar constituents resulted in the emergence of "bees" where previously none had been observed.[2, 4, 6, 42] A possible explanation for these observations is that the wax is *less* soluble in more polar environments, so polar additives cause the existing wax to separate out.[52] As an analogy, if salt is added to a water-alcohol solution, the salt dissolves in the water and the alcohol separates from the mixture. But not all polar molecules will have the same effect; amphiphilic molecules (molecules with both hydrophilic and hydrophobic chemical groups) can act as surfactants or emulsifiers, aiding the dispersion of non-polar waxes in the bitumen and themselves segregating to the surface as monolayers. Fat blooming on chocolate has been cited as an analogy for "bee" structure formation, and emulsifying agents like lecithin in chocolate can inhibit fat blooming.[53]

Surface separation of wax does not preclude the presence of wax in the bulk or of a bulk heterostructure, it only suggests that a solubility limit has been reached. Phase separation can happen both at the surface and in the bulk, and the correlation between crystalline material content and "bee" structures could be an indication of this process.[12, 16] The primary requirement is chemical equilibrium: the chemical potentials of the wax dissolved in the bulk, separated in the bulk, and separated at the surface must all be equal.[52] However, it should be emphasized that the specific morphologies of phase separation in the bulk and at the surface can be different.

3.4 Artifacts due to sample flow and AFM imaging

Unfortunately, some experimental artifacts were impossible to eliminate, such as the fact that AFM imaging itself could affect the surface texture of the imaged area (see ESI Figure S8). Distortion of the specimen after AFM imaging was visible optically and is attributed to local heating of the sample by the AFM laser that is focused on the tip and used to monitor cantilever deflection.[54] AFM images of the same samples from Fig. 4 after 32 days of storage but taken at a different location on each sample showed the same distortions but smaller in height and size. For example, in the sample stored under ambient conditions, the para phase expanded upward in height after 32 days, but the area that was repeatedly imaged during that month exhibited a much larger height increase (*ca*. 25 nm) than a different area imaged only at the end of that month (*ca*. 10 nm). Local heating didn't appear to fundamentally alter how the structures aged or their dependence on humidity but did increase the magnitude or speed of change. The sample stored at 4 °C may have also been susceptible to additional complications due to cyclic thermal strain. To minimize the experimental artifacts, the sample was left for 30 min at room temperature before being removed from the dry jar and imaged because even brief exposure to ambient humidity could introduce artifacts due to water condensation on the cold surface.

The morphology of the "bee" structures is dependent on thermal history and changes with heating and annealing.[9, 10, 13, 55] If the binder sample on glass is tilted while cooling, the binder also flows to one side. Figure 6 shows AFM images demonstrating how this tilt significantly affected both the number and structure of the "bees" at different locations on some samples. The maximum incline angle was approximately 3°. Areas upstream of the flow showed fewer structures and almost no catana phase (Fig. 6b) whereas areas downstream of the flow on another sample experienced severe crowding (Fig. 6c). This result is consistent with a view of the "bee" structures as being thin surface films floating on fluid para phase. If the "bees" possessed a significant depth or volume, then dilution or crowding of the structures would induce extreme counter-flow of para phase matrix in the opposite direction into or out of the area. Counter-flow on this size scale would be possible only for a low viscosity matrix or a very strong driving force such as a large density difference between the matrix and dispersed phases, neither of which is the case in this system.

Flow rate was also observed to decrease with time due to both cooling and the viscoelasticity of the sample. When the flow stopped at high temperature prior to significant bee-structure formation, then new "bees" nucleated and grew normally, and no difference was seen (data not shown). However, if the cooling rate was rapid or the flow continued during or after "bee" formation, then significant structural alterations occurred. In Fig. 6a and 6b, the sample was set at an inclined position after it had already cooled to 70 °C instead of immediately after removal from the oven at 150 °C. Fig. 6a shows typical "bee" structures while Fig. 6b shows a surface morphology in which sample flow depleted the local area of "bees," allowing new structures to nucleate without adequate time to develop catana phase wrinkles. Another

hypothesis is that the flow created tensile strain that negated the native compressive strain ε_{bee} and stretched out the "bees," keeping ε_{bee} below the critical strain for buckling ε_c.

Tapping mode is generally recommended over contact mode for basic AFM imaging of bitumen samples because the lighter tip-sample contact force reduces tip contamination and improves image stability.[40, 56] The contact force in tapping mode is modulated by the amplitude setpoint and was found to have a significant effect on the images as shown in Figure 7. Most images in this study were obtained at light tapping with a setpoint above 75% of the reference value where the phase contrast is typically dominated by topology rather than material properties.[57] As the tip-sample force increased with decreasing setpoint below 75%, the phase contrast of the "bee" structures showed a discontinuous shift coupled with a slight decrease in reported height. This effect is due to the transition from attractive to repulsive tip-sample interactions[57, 58] and can be attributed to the weaker adhesive force of the peri phase.[40] In addition, Fig. 7b shows that high force imaging instantly disrupted the organization of observed fine line structures in the para phase whereas no perturbation was observed for low force. The images were obtained by continuous AFM imaging which captured a frame roughly every 7 min each time a full scan completed and restarted. The para phase lines were previously observed and theorized to be related to creep or contraction of the para phase.[59, 60] In Fig. 7b they appear to be fragmenting like solid nanostructures, and their exact origin is unknown. Repeated imaging at high force did not reveal any progressive alteration of the peri phase. High contrast in the phase image is useful for digital image analysis, but researchers should be cognizant of the potential effects of higher tapping force, especially at elevated temperature. In addition, ascribing material properties to phase contrast is not necessarily straightforward.[57, 61]

4. Conclusions

A detailed AFM microscopy study of bitumen samples under mechanical strain and under different sample preparation and storage conditions leads us to hypothesize that the observed "bee" structures are very thin (*ca*. 10 nm), stiff surface films of crystallized wax that buckle under native compressive strains due to curvature of the growing crystal and differential thermal contraction upon cooling. While not conclusive, the evidence reported herein fully supports this hypothesis. This theory poses significant implications for both current understanding and directions for future work. Firstly, experimental measurements of the mechanical properties of "bee" structures by probe indentation-type methods may be severely confounded if the film is so thin, leading to conflicting data and inaccurate modelling. The "bee" structures also are not necessarily at equilibrium since the wrinkling effect still results in residual stresses that are susceptible to relaxation and creep. Residual stresses may further confound mechanical measurements. Furthermore, improper sample handling or annealing can result in kinetically trapped morphologies and variability.

The properties of a surface film may affect how bitumen ages under environmental exposure. Hydrophobic surface films may block water from absorbing into bitumen while also preventing small polar molecules from leaching out of the bitumen matrix; this in turn could reduce overall bitumen aging. Conversely, the surface films are fragile and may be lost to contact abrasion. Gaps in native surface passivating films can self-repair by migration of more material from the bulk to the surface, but repeated delamination could eventually deplete the bitumen of wax. In other words, two different bitumen samples with and without "bee" structures may chemically age in different ways. On the other hand, the wavelength (λ_o) of the ripples in "bee"

structures could be a promising indicator for the stiffness and thermal expansion coefficient of the para phase resin. Considering that our study showed the para phase as being most susceptible to environmental conditions, such an indicator can be further used to determine the extent of aging in bitumen based on the evolution of microscopic structure. Studies are underway to evaluate how the wavelength of "bees" varies during the aging process.

Acknowledgement

This research is sponsored by the National Science Foundation (Award No: 1150695). The authors are grateful for the support from NSF and the Joint School of Nanoscience and Nanoengineering as well as the State of North Carolina. The authors are also very grateful to Oleg Butyaev, Sergei Magonov, and Marko Surtchev of NT-MDT for useful discussions and preliminary testing. The contents of this paper reflect the view of the authors, who are responsible for the facts and the accuracy of the data presented. This paper does not constitute a standard, specification, or regulation.

References

1. L. Loeber, O. Sutton, J. Morel, J. M. Valleton and G. Muller, *J. Microsc.-Oxford*, 1996, **182**, 32-39.
2. J. F. Masson, V. Leblond and J. Margeson, *J. Microsc.-Oxford*, 2006, **221**, 17-29.
3. X. K. Yu, N. A. Burnham and M. J. Tao, *Adv. Colloid Interface Sci.*, 2015, **218**, 17-33.
4. A. Jäger, R. Lackner, C. Eisenmenger-Sittner and R. Blab, *Road Mater. Pavement Design*, 2004, **5**, 9-24.
5. S.-p. Wu, L. Pang, L.-t. Mo, Y.-c. Chen and G.-j. Zhu, *Construct. Build. Mater.*, 2009, **23**, 1005-1010.
6. H. L. Zhang, H. C. Wang and J. Y. Yu, *J. Microsc.*, 2011, **242**, 37-45.
7. A. Schmets, N. Kringos, T. Pauli, P. Redelius and T. Scarpas, *Int. J. Pavement Eng.*, 2010, **11**, 555-563.
8. P. K. Das, N. Kringos, V. Wallqvist and B. Birgisson, *Road Mater. Pavement Design*, 2013, **14**, 25-37.
9. M. B. De Moraes, R. B. Pereira, R. A. Simao and L. F. M. Leite, *J. Microsc.*, 2010, **239**, 46-53.
10. H. Soenen, J. Besamusca, H. R. Fischer, L. D. Poulikakos, J.-P. Planche, P. K. Das, N. Kringos, J. R. A. Grenfell, X. Lu and E. Chailleux, *Mater. Struct.*, 2014, **47**, 1205-1220.
11. .
12. A. T. Pauli, R. W. Grimes, A. G. Beemer, T. F. Turner and J. F. Branthaver, *Int. J. Pavement Eng.*, 2011, **12**, 291-309.
13. S. N. Nahar, A. J. M. Schmets, A. Scarpas and G. Schitter, *Eur. Polym. J.*, 2013, **49**, 1964-1974.
14. E. D. Sourty, A. Y. Tamminga, M. A. J. Michels, W. P. Vellinga and H. E. H. Meijer, *J. Microsc.*, 2011, **241**, 132-146.
15. H. R. Fischer, E. C. Dillingh and C. G. M. Hermse, *Road Mater. Pavement Design*, 2013, **15**, 1-15.
16. Q. Qin, M. J. Farrar, A. T. Pauli and J. J. Adams, *Fuel*, 2014, **115**, 416-425.
17. H. R. Fischer and E. C. Dillingh, *Fuel*, 2014, **118**, 365-368.
18. S. dos Santos, M. N. Partl and L. D. Poulikakos, *Construct. Build. Mater.*, 2014, **71**, 618-627.
19. S. N. Nahar, M. Mohajeri, A. J. M. Schmets, A. Scarpas, M. F. van de Ven and G. Schitter, Transportation Research Board 92nd Annual Meeting, 2013.

20. A. L. Lyne, V. Wallqvist, M. W. Rutland, P. Claesson and B. Birgisson, *J. Mater. Sci.*, 2013, **48**, 6970-6976.
21. T. Pauli, W. Grimes, J. Beiswenger and A. J. M. Schmets, *J. Mater. Civil Eng.*, 2015, **27**, C4014001.
22. R. Mehta, W. Keawwattana, A. L. Guenthner and T. Kyu, *Phys. Rev. E*, 2004, **69**, 061802.
23. A. Toda, M. Okamura, M. Hikosaka and Y. Nakagawa, *Polymer*, 2005, **46**, 8708-8716.
24. M. Kane, M. Djabourov, J. L. Volle, J. P. Lechaire and G. Frebourg, *Fuel*, 2003, **82**, 127-135.
25. M. Zbik, R. G. Horn and N. Shaw, *Colloids and Surfaces A: Physicochem. Eng. Aspects*, 2006, **287**, 139-146.
26. R. J. Young and P. A. Lovell, *Introduction to Polymers*, 2nd edn., Chapman & Hall, New York, 1991.
27. H. Q. Jiang, D. Y. Khang, J. Z. Song, Y. G. Sun, Y. G. Huang and J. A. Rogers, *Proc. Natl. Acad. Sci. U.S.A.*, 2007, **104**, 15607-15612.
28. R. Huang and S. H. Im, *Phys. Rev. E*, 2006, **74**, 026214.
29. S. H. Im and R. Huang, *J. Appl. Mech.*, 2005, **72**, 955-961.
30. R. Huang, *J. Mech. Phys. Solids*, 2005, **53**, 63-89.
31. H. R. Fischer and B. Dillingh, *Road Mater. Pavement Design*, 2015, **16**, 31-45.
32. S. N. Nahar, A. J. M. Schmets, A. Scarpas and G. Schitter, *Eur. Polymer J.*, 2014, **56**, 17-25.
33. S. Zhao, S. N. Nahar, A. J. M. Schmets, B. Huang, X. Shu and T. Scarpas, *Road Mater. Pavement Design*, 2015, **16**, 21-38.
34. P. K. Das, N. Kringos and B. Birgisson, *J. Microsc.*, 2014, **254**, 95-107.
35. D. Oldham, A. M. Hung and E. H. Fini, *in preparation*.
36. R. Jahangir, D. Little and A. Bhasin, *Int. J. Pavement Eng.*, 2015, **16**, 337-349.
37. E. Cerda and L. Mahadevan, *Phys. Rev. Lett.*, 2003, **90**, 074302.
38. A. Motamed, A. Bhasin and K. Liechti, *Mech. Time-Depend. Mater.*, 2012, **16**, 145-167.
39. M. C. Strus, A. Raman, C. S. Han and C. V. Nguyen, *Nanotechnology*, 2005, **16**, 2482.
40. X. K. Yu, N. A. Burnham, R. B. Mallick and M. J. Tao, *Fuel*, 2013, **113**, 443-447.
41. H. Fischer, H. Stadler and N. Erina, *J. Microsc.*, 2013, **250**, 210-217.
42. X. K. Yu, M. Zaumanis, S. dos Santos and L. D. Poulikakos, *Fuel*, 2014, **135**, 162-171.
43. E. R. Dourado, R. A. Simao and L. F. M. Leite, *J. Microsc.*, 2012, **245**, 119-128.
44. R. G. Allen, D. N. Little and A. Bhasin, *J. Mater. Civil Eng.*, 2012, **24**, 1317-1327.
45. A. Jäger, R. Lackner and J. Eberhardsteiner, *Meccanica*, 2007, **42**, 293-306.
46. C. L. Choy, Y. W. Wong, G. W. Yang and T. Kanamoto, *J. Polym. Sci. Polym. Phys.*, 1999, **37**, 3359-3367.
47. P. F. Li, L. Hu, A. J. H. McGaughey and S. Shen, *Adv. Mater.*, 2014, **26**, 1065-1070.
48. S. Kim, *J. Mater. Civil Eng.*, 2005, **17**, 632-639.
49. D. W. van Krevelen, *Properties of Polymers*, 3rd edn., Elsevier, San Diego, 1997.
50. J. B. Lambert, S. Gronert, H. F. Shurvell and D. A. Lightner, *Organic Structural Spectroscopy*, 2nd edn., Prentice Hall, New York, 2011.
51. R. G. Allen, D. N. Little, A. Bhasin and C. J. Glover, *Int. J. Pavement Eng.*, 2014, **15**, 9-22.
52. J. N. Israelachvili, *Intermolecular and Surface Forces*, 3rd edn., Academic Press, San Diego, 2011.
53. P. Lonchampt and R. W. Hartel, *Euro. J. Lipid Sci. Technol.*, 2004, **106**, 241-274.
54. A. T. Pauli and W. Grimes, in *Abstr. Pap. Amer. Chem. Soc.*, 2003, vol. 225, pp. U422-U422.
55. J. F. Masson, V. Leblond, J. Margeson and S. Bundalo-Perc, *J. Microsc.*, 2007, **227**, 191-202.
56. S. N. Nahar, B. Dillingh, S. M. J. G. Erkens, A. J. M. Schmets, H. R. Fischer, A. Scarpas and G. Schitter, in *Transportation Research Board 92nd Annual Meeting*, Transportation Research Board, Washington, USA, 2013.
57. X. Chen, C. J. Roberts, J. Zhang, M. C. Davies and S. J. B. Tendler, *Surf. Sci.*, 2002, **519**, L593-L598.

58. X. Chen, M. C. Davies, C. J. Roberts, S. J. B. Tendler, P. M. Williams and N. A. Burnham, *Surf. Sci.*, 2000, **460**, 292-300.
59. I. Menapace, E. Masad, D. Little, E. Kassem and A. Bhasin, in *Sustainability, Eco-efficiency, and Conservation in Transportation Infrastructure Asset Management*, eds. M. Losa and T. Papagiannakis, Taylor & Francis Group, London, 2014.
60. I. Menapace, E. Masad, A. Bhasin and D. Little, *Road Mater. Pavement Design*, 2015, **16**, 2-20.
61. O. P. Behrend, L. Odoni, J. L. Loubet and N. A. Burnham, *Appl. Phys. Lett.*, 1999, **75**, 2551-2553.

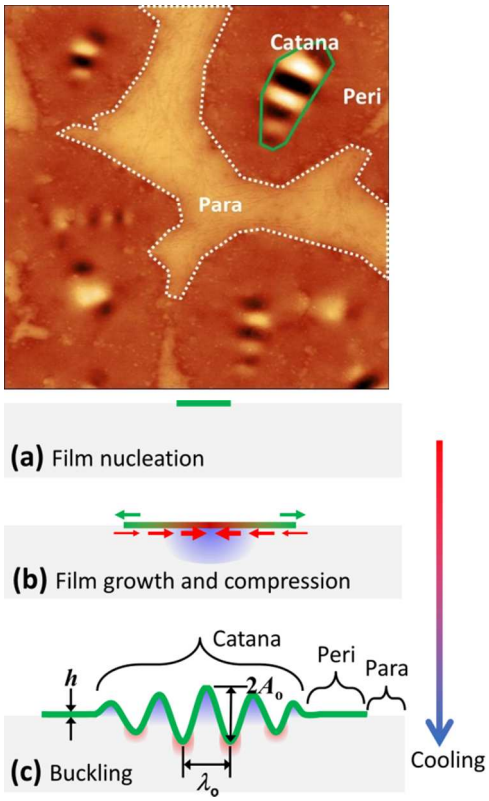

Figure 1. An example AFM height image (5 μm scan) of three topologically distinct areas observed on a bitumen surface and a schematic illustration of the hypothesized process of "bee" formation: (a) nucleation and growth of a paraffin wax thin film, (b) compression of the film due to thermal contraction of the underlying bitumen and curvature of the growing crystal, and (c) buckling of the film at a critical strain. Approximate regions of compressive and tensile strain in the schematic are shaded red and blue, respectively.

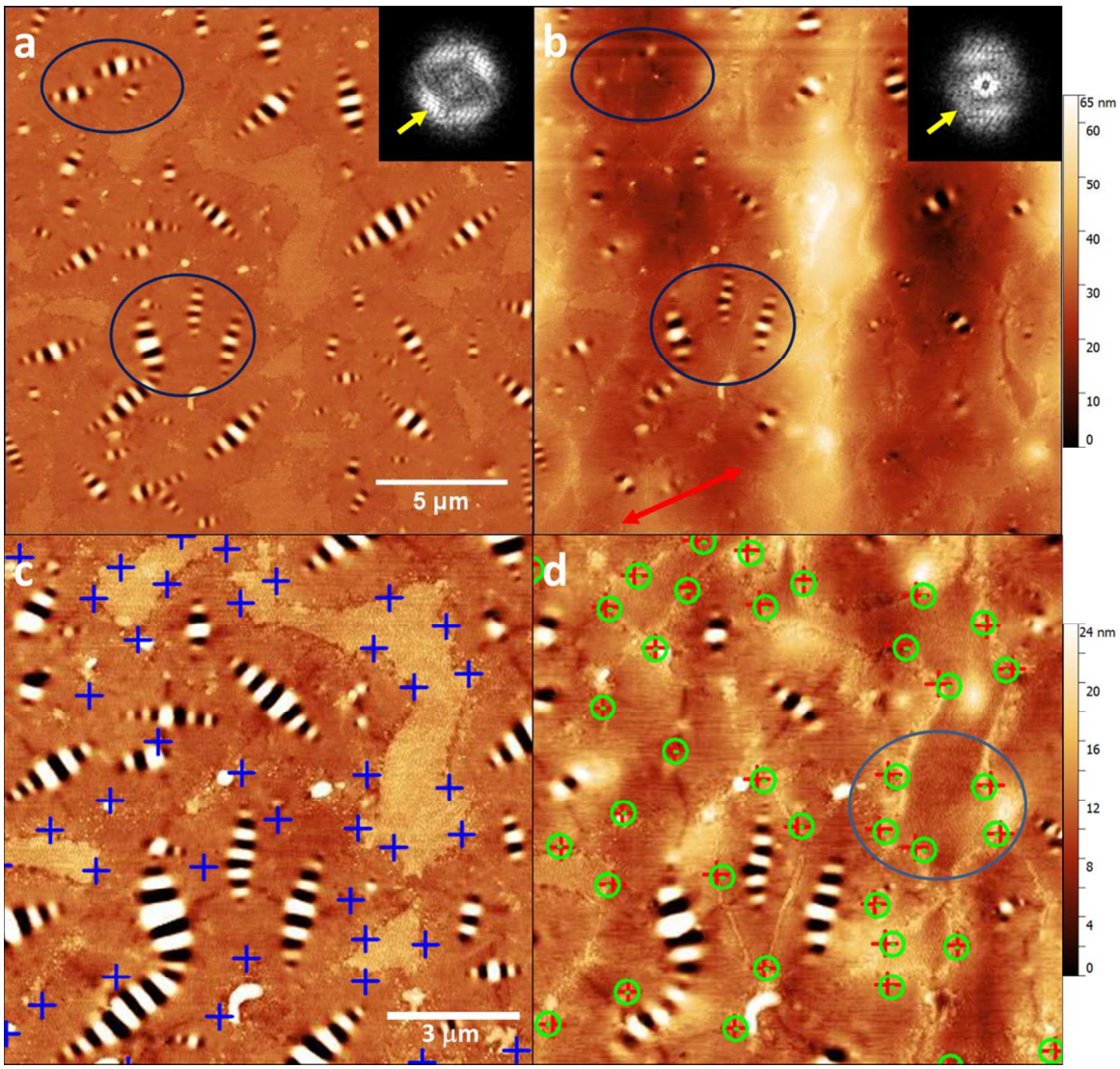

Figure 2. (a, b) AFM topography images of a binder sample (a) before and (b) after stretching in the horizontal direction. Comparison of "bee" structures (blue circles) and FFT analysis (insets) shows selective elimination of "bees" oriented more parallel to the stretching direction. Scale bar and false color height ruler applies to both images. (c, d) The two images were flattened and contrasted more severely to facilitate identification of fine features. A set of spots that could be matched between the "before" (blue crosses) and "after" images (red crosses) were identified. The "before" coordinates were transformed to yield a set of predicted coordinates (green circles) that model the result of a uniform plane strain (see ESI Figure S3 for full image). The average strain in this location is calculated to be 7.4% at an angle of 24° (red arrow). Deviations between the predicted and real coordinates (light blue oval) provide additional information about local strain distribution.

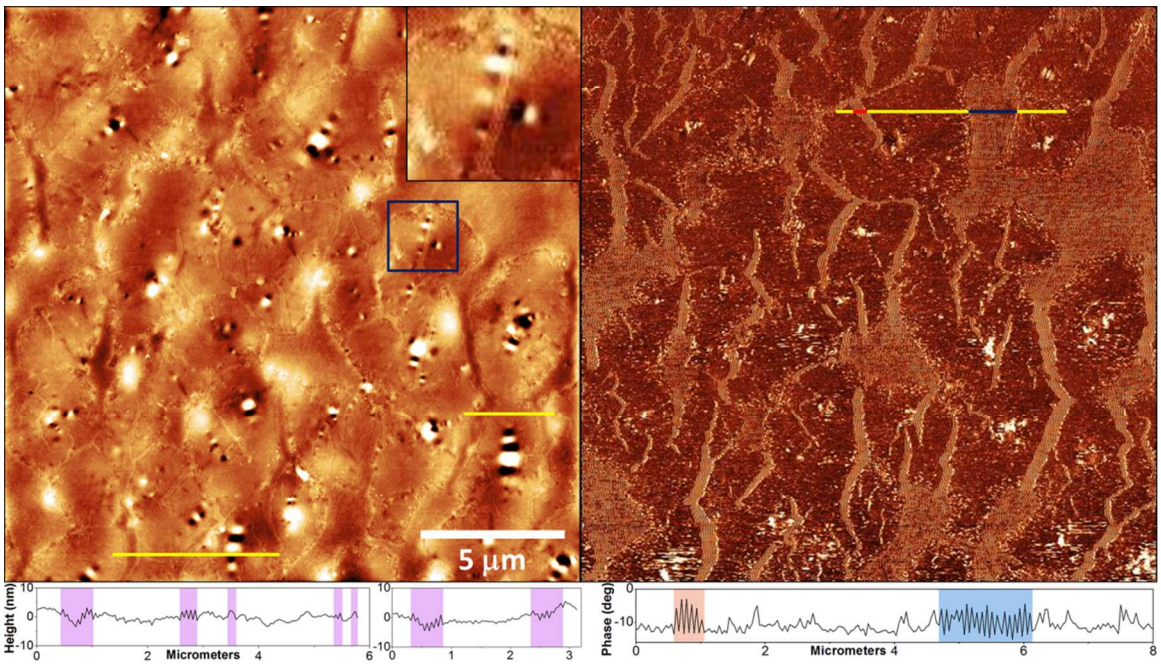

Figure 3. Flattened topography (left) and phase (right) images show the effect of higher strain in fracturing the "bee" structures. The images are of a different location on the same specimen as in Fig. 2. Inset image and line profile plots show that the topography within the cracks (highlighted sections of profile plots) appears shallow or even raised above the surrounding peri phase. This and other features are discussed in more detail in the text. False color height scale for the topography image is 20 nm. See ESI Figures S4 and S5 for larger, alternate versions of this topography image.

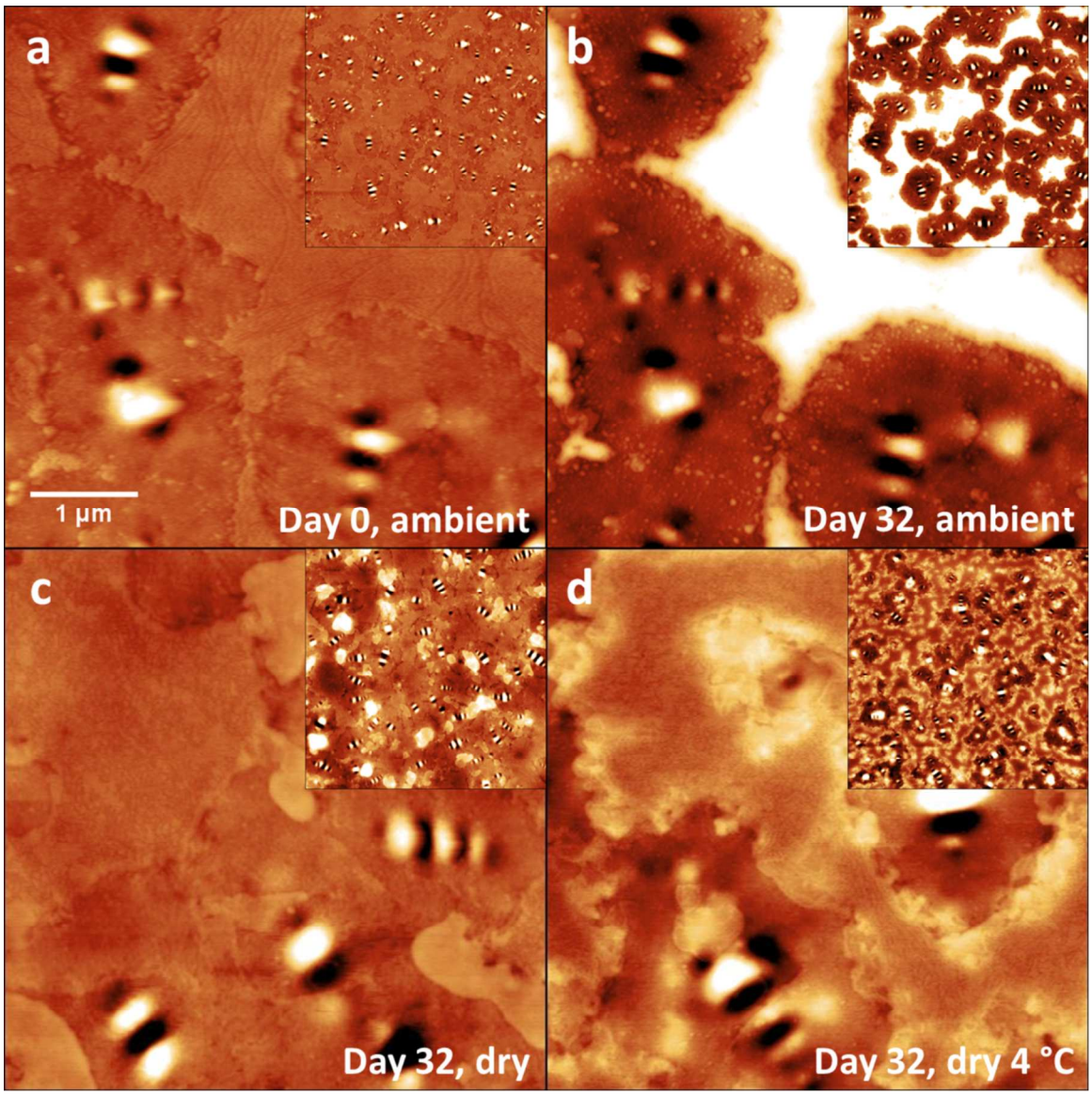

Figure 4. AFM topography images show the effect of storage conditions on the evolution of bee-like structures after 32 days. The samples were stored under (a, b) ambient temperature and humidity (22 °C, 50% humidity), (c) room temperature in dry air, or (d) 4°C in dry air. Scale bar applies to all images, insets are 20 µm square areas, and the height scale for all images is 25 nm.

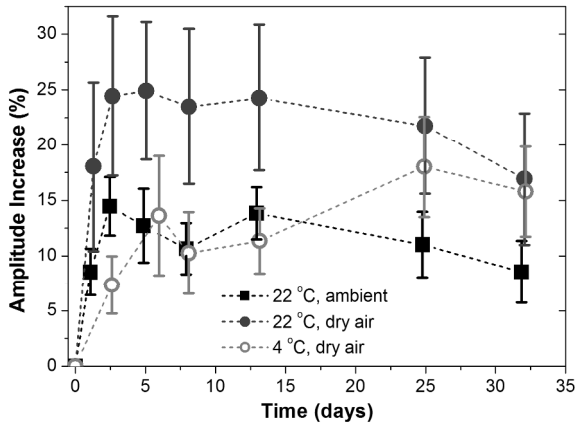

Figure 5. Change in amplitude the "bee" structures plotted as functions of time and storage conditions. Error bars are 5% confidence interval.

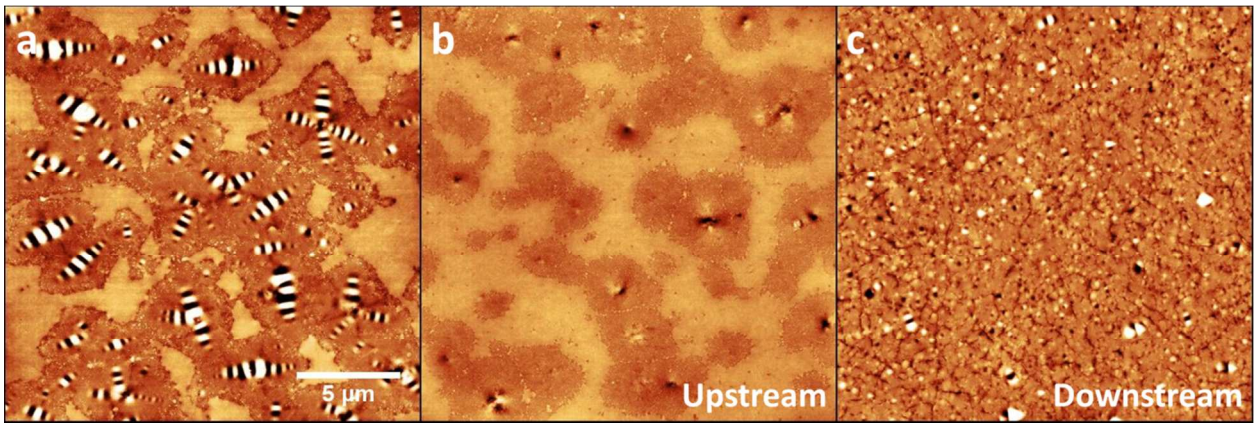

Figure 6. AFM topography images of (a) typical "bee" structures and (b, c) different textures that resulted from flow during cooling. The imaged areas are (b) upstream or (c) downstream of the flow. Images (a) and (b) are of two locations only 2 mm apart on the same specimen. Height scale is 20 nm and scale bar applies to all images.

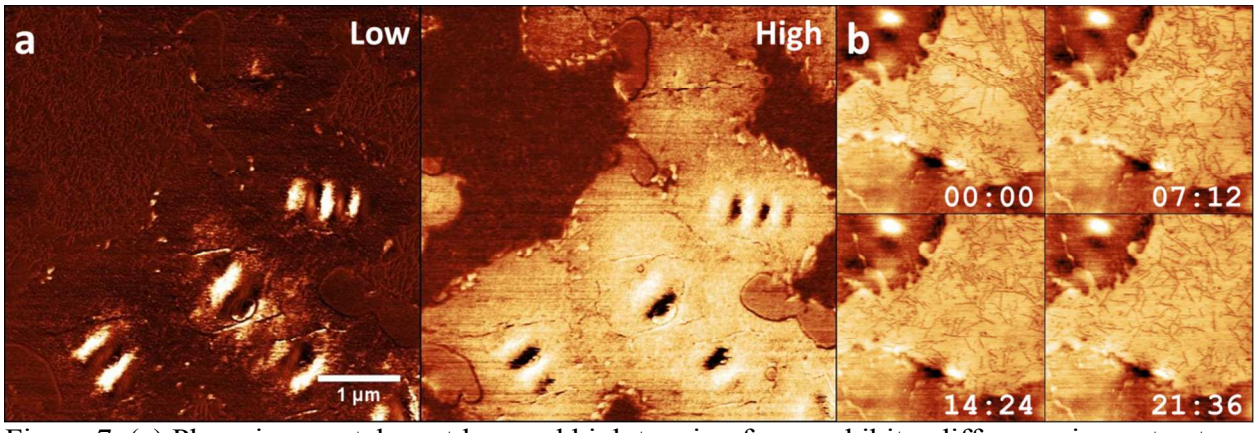

Figure 7. (a) Phase images taken at low and high tapping force exhibit a difference in contrast. The images were taken at the same location as in Fig. 4c. (b) Topography images of the para

phase between the “bees” at high force show disruption of the observed line features with continuous imaging. The relative time at which each image was captured is labelled (mm:ss). Scan size is 2 μm and height scale is 9 nm.